Influence of Heat Release in a Premixed Flame on Weakly Turbulent Flow of Unburned Gas: A DNS Study

Andrei N. Lipatnikov, Jerzy Chomiak,
Department of Applied Mechanics, Chalmers University of Technology
Gothenburg, Sweden

Vladimir A. Sabelnikov,
ONERA - The French Aerospace Lab.,
Palaiseau, France

Shinnosuke Nishiki,
Department of Mechanical Engineering, Kagoshima University,
Kagoshima, Japan

Tatsuya Hasegawa,
EcoTopia Science Institute, Nagoya University,
Nagoya, Japan

1 Introduction

The seminal work by Karlovitz et al. [1] initiated research into the influence of premixed combustion on turbulent flow and the so-called flame-generated turbulence. Progress obtained in this area is reviewed elsewhere [2], but the focus of the vast majority of studies of the flame-generated turbulence has yet been placed on the flow downstream the instantaneous flame front within the mean flame brush. Only recently, Swaminathan and Grout [3] found that, due to density variations, scalar gradients within the instantaneous flame front could preferentially be aligned with the direction of the most expansive strain rate, whereas scalar gradients align preferentially with the most compressive strain rate in a constant-density turbulent flow. Subsequently, the alignment issue was addressed in a couple of DNS and experimental studies, which confirmed the aforementioned finding, e.g. see Refs. [4,5]. However, little is yet known about the influence of combustion on the constant-density flow of unburned gas upstream the instantaneous flame front. In the past year, the present authors [6] analyzed the Nagoya DNS database [7,8] and showed that acceleration of the unburned gas by combustion-induced pressure gradient yielded unburned mixture fingers that deeply intruded into the products, thus, significantly increasing flame surface area, turbulent burning rate, and mean flame brush thickness. The present work aims at further studying the Nagoya DNS database in order to reveal more effects associated with the influence of heat release due to premixed combustion on the near-field upstream constant-density turbulent flow of unburned gas, especially strain rate and vorticity. Far-field noise, which is very sensitive to the acoustic boundary conditions, is beyond the scope of the paper.

Correspondence to: lipatn@chalmers.se

2 DNS Attributes

Because DNSs addressed here were discussed in detail elsewhere [6-8], we restrict ourselves to a brief summary of the simulations. The DNSs were compressible and dealt with statistically planar, 1D, adiabatic premixed flames modeled by unsteady 3D continuity, Navier–Stokes, and energy equations, as well as the ideal gas state equation. Combustion chemistry was reduced to a single reaction.
The computational domain was a rectangular 8×4×4 mm, and was resolved using a uniform mesh of $512\times128\times128$ points. Homogeneous isotropic turbulence (rms velocity u'=0.53 m/s, integral length scale L=3.5 mm, Kolmogorov length scale η=0.14 mm, and Re_t=96 [7,8]) was generated in a separate box, injected into the computational domain with a mean velocity U at $x=0$, and decayed along the direction x of the mean flow. The flow was periodic in y and z directions.
At an initial instant, a planar laminar flame was embedded into statistically the same turbulence assigned for the velocity field in the entire computational domain. Three cases characterized by three different density ratios $\sigma=\rho_u/\rho_b$ were investigated, see Table 1, where S_L is the laminar flame speed, $\delta_L=(T_b-T_u)/\max|dT/dx|$ is the laminar flame thickness, T is the temperature, κ_u is the heat diffusivity of unburned gas, subscripts u and b designate unburned and burned mixture, respectively. In the following, we will restrict ourselves to comparing results obtained in cases H and L, characterized by the highest and lowest density ratio, respectively.

Table 1: Flame characteristics

	σ	S_L, m/s	δ_L, mm	κ_u/S_L, mm	S_t, m/s
Case H	7.53	0.600	0.217	0.037	1.13
Case M	5.0	0.523	0.191	0.042	1.00
Case L	2.5	0.416	0.158	0.053	0.74

During the simulations, the inflow velocity was increased at two instants, i.e. $U(0\le t<t_1)=S_L<U(t_1\le t<t_2)<U(t_2\le t)=S_t$ in order to keep the mean flame brush in the computational domain till the end t_3 of the simulations. Results reported here were obtained at $t\ge t_2$ and constant U. Both time-dependent mean quantities $\overline{q}(t)$ averaged over transverse yz-planes and mean quantities $\langle q\rangle$ averaged also over time interval $t_2\le t\le t_3$, which was about $1.5L/u'$, were evaluated. Computed dependencies of mean quantities on the axial coordinate x were transformed into dependencies of these quantities on the Reynolds-averaged combustion progress variable $\langle c\rangle$ using the profiles of $\langle c\rangle(x)$, where $c=(T_b-T_u)/(T_b-T_u)$.

3 Results and Discussion

Figure 1 shows the evolution of the so-called Q-criterion

$$Q=\frac{1}{2}\left(\Omega_{ij}\Omega_{ij}-S_{ij}S_{ij}\right)=\frac{1}{8}\left[\left(\frac{\partial u_i}{\partial x_j}-\frac{\partial u_j}{\partial x_i}\right)\left(\frac{\partial u_i}{\partial x_j}-\frac{\partial u_j}{\partial x_i}\right)-\left(\frac{\partial u_i}{\partial x_j}+\frac{\partial u_j}{\partial x_i}\right)\left(\frac{\partial u_i}{\partial x_j}+\frac{\partial u_j}{\partial x_i}\right)\right],$$

which is widely used to characterize relative magnitudes of strain rate $\mathbf{S}$ and vorticity $\mathbf{\Omega}$ tensors in a turbulent flow. Here, the summation convention applies for the repeated indexes i and j. Positive (negative) values of Q are associated with the predominance of vorticity (strain rate) in the flow. Shown in the left Fig. 1 are the values of Q averaged (i) in the vicinity of a leading point, i.e. over a square such that $x=x^*(t)$, $|y-y^*(t)|\le h_y$, $|z-z^*(t)|\le h_z$, see dashed lines, and (ii) over entire leading plane $x=x^*(t)$, see solid lines, at various instants. The leading point $\mathbf{x}^*(t)=\{x^*(t),y^*(t),z^*(t)\}$ was found using the following two constraints; $c(x^*,y^*,z^*,t)\ge0.05$, but $c(x,y,z,t)<0.05$ in all points $\{x<x^*(t),y,z\}$ at the same instant t. Accordingly, both the leading-point and the leading-plane Q were evaluated in the unburned gas. Here, $h_y=h_z$ are grid steps in the transverse directions, i.e. the aforementioned square

includes the leading point and eight neighboring points characterized by $j=j^*-1$, j^*, or j^*+1 and $k=k^*-1$, k^*, or k^*+1. Results computed in cases H and L are roughly associated with $t<21$ ms and $t>21$ ms, respectively. Shown in the right Fig. 1 are the probabilities of positive (solid lines) and negative (dashed lines) Q on the instantaneous flame-front surface $x=x_f(y,z,t)$ that was found using the following two constraints; (i) $c[x_i=x_f(y_j,z_k,t),y_j,z_k,t]\geq 0.05$, but (ii) $c(x_i,y_j,z_k,t)<0.05$ in an interval of $\{0\leq x_i<x_f(y_j,z_k,t),y=y_j,z=z_k\}$ at the same t.

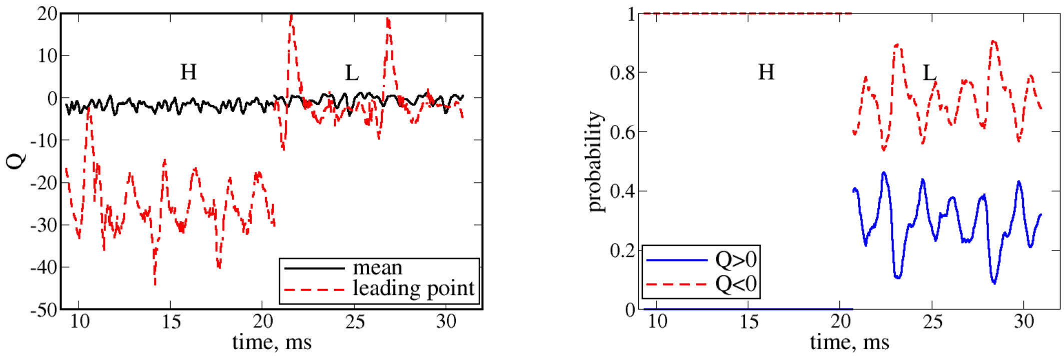

Figure 1. Evolution of Q-criterion evaluated in the unburned gas. Left: Q-criterion averaged over the leading planes $x=x^*(t)$, see solid lines, and in the vicinity of the leading points, see dashed lines. Right: probabilities of $Q>0$, see solid lines, and $Q<0$, see dashed lines, conditioned on the instantaneous flame-front surface $x=x_f(y,z,t)$.

Figure 1 indicates the following trends. First, the behavior of Q averaged over the leading plane is similar in cases H and L, see black solid lines, while the density ratio is lower by a factor of about three in the latter case. Second, Q averaged in the vicinity of the leading point is statistically lower than Q averaged over the leading plane, with the difference being much more pronounced in case H characterized by a higher density ratio. Third, Q is predominately negative not only in the vicinity of the leading point, but also near the entire instantaneous flame front, with the probability of finding positive Q at the front vanishing in case H and being low in case L, see blue solid lines. These trends imply that, under conditions of the present DNSs, (i) the flame front propagates upstream through flow regions characterized locally by higher strain rates when compared to vorticity and (ii) heat release affects the upstream flow by yielding such local regions.

Because flow perturbations propagate upstream due to pressure perturbations, results shown in Fig, 1 imply that combustion should affect pressure field upstream the flame front. Indeed, the left Fig. 2 indicates that pressure conditioned on unburned front edge is statistically higher than the pressure conditioned on unburned gas at the same x, with the difference being more pronounced at the leading edge of the mean flame brush and being significantly increased by the density ratio, cf. dashed and solid lines. The right Fig. 2 indicates that pressure evaluate locally at the leading point is statistically higher than the pressure averaged over the leading plane. These results imply that local high-pressure regions caused by heat release in the instantaneous flame front push away the flow upstream the front and promote the upstream propagation of the front, in line with qualitative discussion in Appendix to Ref. [2], see Fig. 59 therein. In the case of laminar burning, such a physical mechanism was discovered by Darrieus and Landau who independently predicted the hydrodynamic instability of premixed flames, e.g. see the aforementioned review paper [2]. Because pressure perturbations cause potential perturbations of the upstream constant-density flow of unburned gas (if ρ=const, then, the pressure gradient term vanishes after taking the curl of the Navier-Stokes equations), the discussed pressure perturbations increase the negative (strain rate) component of the Q-factor, in line with the DNS results reported in Fig. 1.

Figure 3 shows 2D normalized spectra $e(k,\langle c\rangle)$ for the transverse components of the velocity vector, obtained in unburned gas at various $\langle c\rangle(x)$ in cases H and L. The spectra were computed as follows

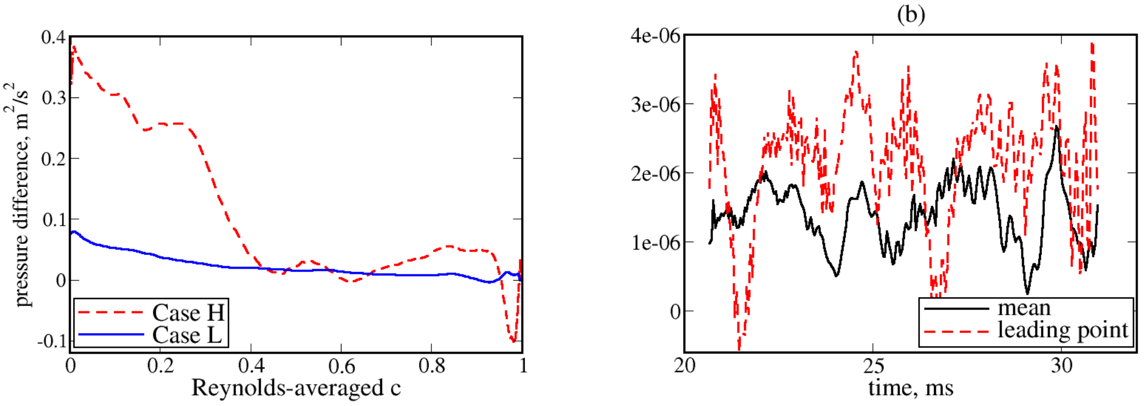

Figure 2. Left: Difference between pressures conditioned on unburned flame-front edge (0.01<c<0.05) and unburned gas (c<0.05). Right: relative pressure difference $p(\mathbf{x},t)/p_{in}(t)$-1 averaged over the leading plane $x=x^*(t)$, see solid lines, and evaluated at the leading point, see dashed lines. Here, the pressure $p_{in}(t)$ is averaged over the inlet.

$$e\left(k,\langle c\rangle\right)=\frac{\int_0^{2\pi}\left[\Phi_{yy}\left(k,\varphi,\langle c\rangle\right)+\Phi_{zz}\left(k,\varphi,\langle c\rangle\right)\right]d\varphi}{\lambda_u\left(\langle c\rangle\right)\left[R_{yy}\left(0,\langle c\rangle\right)+R_{zz}\left(0,\langle c\rangle\right)\right]},$$

$$\Phi_{jj}\left(k,\varphi,\langle c\rangle\right)=\frac{4}{(2\pi)^2}\int_0^{\Lambda_y/2}\int_0^{\Lambda_z/2}\langle R_{jj}\rangle\left(\langle c\rangle,y,z\right)\cos\left(ky\cos\varphi+kz\sin\varphi\right)dz\,dy\,,$$

where $u_u'\left(\langle c\rangle\right)$, $\langle\varepsilon\rangle_u\left(\langle c\rangle\right)$, and $\lambda_u\left(\langle c\rangle\right)=\lambda_0\sqrt{\langle\varepsilon\rangle_0/\langle\varepsilon\rangle_u\left(\langle c\rangle\right)}\,u_u'\left(\langle c\rangle\right)/u_0'$ are the rms turbulent velocity, dissipation rate, and Taylor length scale conditioned on unburned gas and averaged over transverse planes characterized by various $\langle c\rangle$ specified in figure legends, while u_0', $\langle\varepsilon\rangle_0$, and λ_0 are the counterpart quantities averaged over the inlet plane. The correlations $<R_{jj}>$ were evaluated (i) for various vectors **r** normal to the x-axis, (ii) for the y-th or z-th component of the velocity vector, (iii) in the unburned gas (c≤0.01), and (iv) were averaged over transverse planes characterized by various <c>.

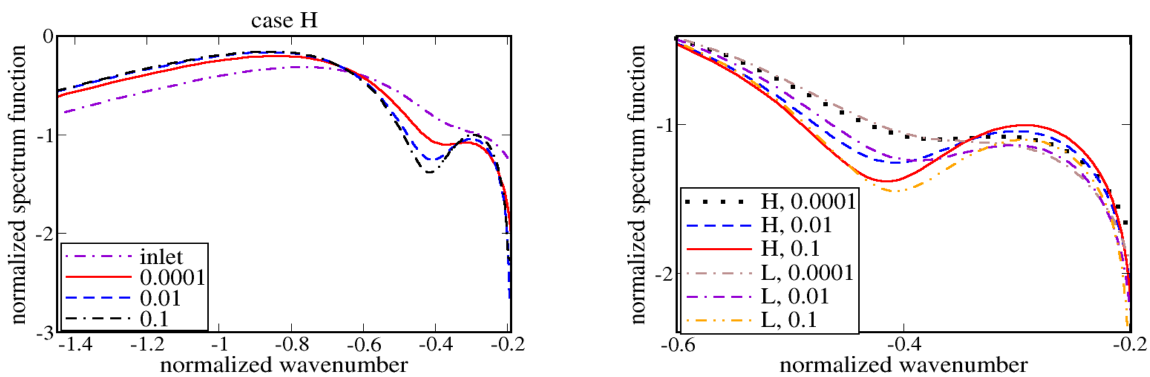

Figure 3. Normalized spectra $e(k,<c>)$ of transverse components of the velocity vector, evaluated in cases H (left and right) and L (only right) in unburned gas at various $x(<c>)$, with $<c>$ being specified in legends. The spectra are shown in the logarithmic scale, i.e. lg$e$ vs. lg($k\lambda_u/2\pi$).

When compared to the inlet spectrum, see violet dotted-dashed line in the left Fig. 3, substantial damping and enhancement of fluctuations of transverse velocity components are clearly visible in wavelengths near $2.6\lambda_u$ and $1.8\lambda_u \approx 1$ mm, respectively. Different amplification of these fluctuations indicates that flow perturbations driven by heat release depend not only on energy, as assumed in the vast majority of combustion theories, but also on the length scale. An efficiency factor associated with the length scale is highly variable. The location $1.8\lambda_u(<c>)$ of the "small-scale" peak of the spectrum is weakly affected by variations in $<c>$, whereas the relative (with respect to the local minimum of the spectrum observed at a lower wavenumber k) peak magnitude is increased by $<c>$ within the leading part of the mean flame brush, i.e. if $<c>$ is about 0.1 or lower. Further increase in $<c>$ affects the relative magnitude weakly (not shown). The same trends are reported in the right Fig. 3 using a larger scale. The small-scale spectrum peaks are observed even in case L characterized by a low density ratio, but the local peak magnitude is higher in case H when compared to case L.

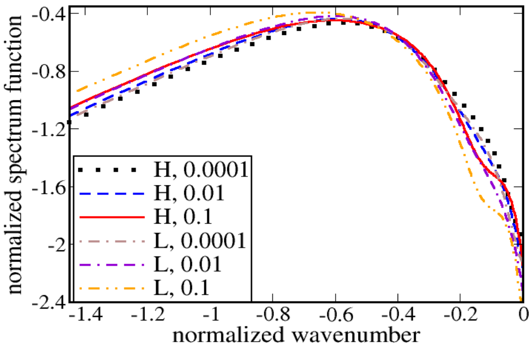

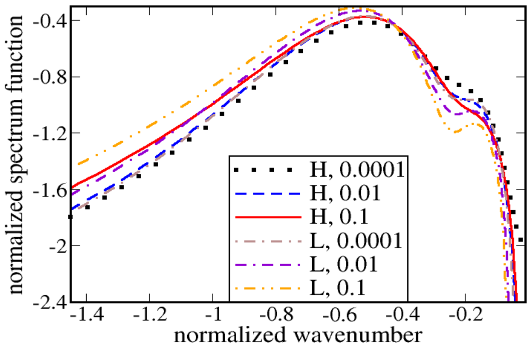

Figure 4. Normalized spectra $v(k,<c>)$ of transverse (left) and axial (right) components of the vorticity vector, evaluated in cases H and L at various $x(<c>)$, with $<c>$ being specified in legends. The spectra are shown in the logarithmic scale, i.e. lg$v$ vs. lg$(k\lambda_u/2\pi)$.

The left Fig. 4 does not show such peaks in the normalized spectra for transverse components of the vorticity vector $\boldsymbol{\omega} = \nabla \times \mathbf{u}$. Comparison of Figs. 3 and 4 implies that the small-scale spectrum peaks are associated with potential flow perturbations caused by pressure perturbations. The latter perturbations result from heat release fluctuations due to motion of the instantaneous flame front and change of its surface area. Nevertheless, the right Fig. 4 indicates similar local peaks in the normalized spectra for the axial component ω_x of $\boldsymbol{\omega}$, but the effect is substantially less pronounced when compared to the velocity spectra and the peaks are observed at larger k.

Figure 5 shows dependencies of mean cosines between the local normal $\mathbf{n}_w$ to the reaction surface and eigenvectors $\boldsymbol{\alpha}$, $\boldsymbol{\beta}$, and $\boldsymbol{\gamma}$ of the rate-of-strain tensor $\mathbf{S}$ on the distance r from the reaction surface $x=x_w(y,z,t)$, with $c(r)$ being a decreasing function. The reaction surface is associated with the lowest x_i such that $c(x_{i-1},y,z) \le c_w \le c(x_i,y,z)$, where c_w=0.89 in order for $W(c)$ to peak at $c=c_w$. In line with the finding by Swaminathan and Grout [3], the local normal vector $\mathbf{n}_w$ aligns preferentially with the most expansive strain rate close to the reaction surface, i.e. within the preheat zone of the instantaneous flame front. When a distance r from the reaction surface is increased, the preferential alignment is reduced and vanishes if r is on the order of $2\delta_L$. Such an effect is not surprising, but, contrary to common expectations, the preferential alignment of $\mathbf{n}_w$ with the most compressive strain rate is not observed in the unburned gas in the vicinity of the front. Although red curves have local maxima at r=0.4-0.7 mm, the effect is weak. The lack of the preferential alignment of $\mathbf{n}_w$ with the most compressive strain rate near the unburned edge of the front could be associated either with the weakness of the turbulence in the present simulations or with the influence of the heat release in the front on the upstream turbulent flow of unburned gas.

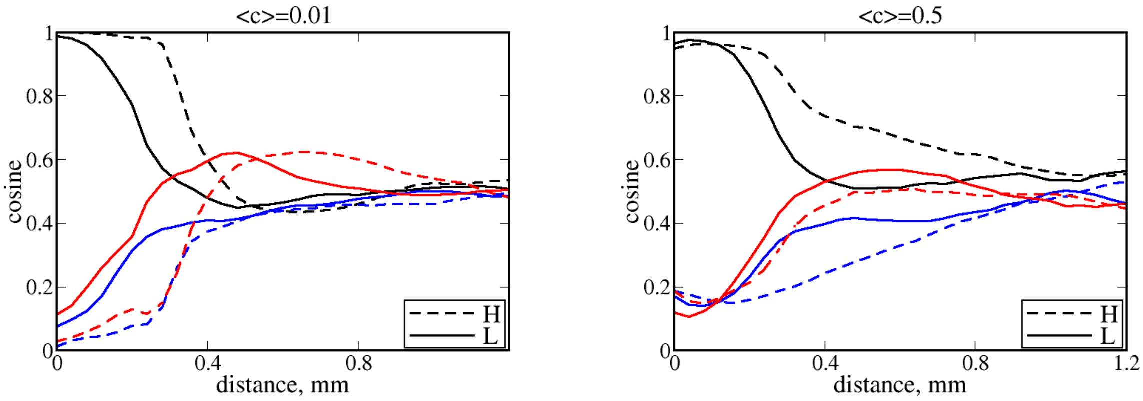

Figure 5. Mean cosines between the local normal $\mathbf{n}_w$ to the reaction surface and eigenvectors $\boldsymbol{\alpha}$, $\boldsymbol{\beta}$, and $\boldsymbol{\gamma}$ of the rate-of-strain tensor $\mathbf{S}$ vs. the distance r from the reaction surface, with $c(r)<c(0)$. Eigenvalues satisfy a constraint of $\alpha\geq\beta\geq\gamma$. Black (red) lines show results associated with the most expansive (compressive) strain rate.

4 Conclusions

Under conditions of the present DNSs, heat release in flame fronts substantially perturbs the pressure field and upstream fluctuating flow of unburned gas and yields local regions characterized by higher strain rates when compared to vorticity, with the flame front preferentially propagating upstream through such regions. Such a scenario differs substantially from the classical paradigm of an increase in the area of the surface of a passive front by turbulent stretching. Further studies of premixed burning in more intense turbulence can provide a deeper insight into the main driving forces of premixed turbulent combustion and conditions under that the Kolmogorov theory of turbulence could be appropriate for characterizing the flow of unburned gas within a premixed turbulent flame brush.

References

[1] Karlovitz B, Denniston, DW, Wells, FE (1951). Investigation of turbulent flames. J. Chem. Phys. 19: 547.

[2] Lipatnikov AN, Chomiak J (2010). Effects of premixed flames on turbulence and turbulent scalar transport. Prog. Energy Combust. Sci. 36: 1.

[3] Swaminathan N, Grout RW (2006). Interaction of turbulence and scalar fields in premixed flames. Phys. Fluids 18: 045102.

[4] Hartung G et al. (2008). Effect of heat release on turbulence and scalar-turbulence interaction in premixed combustion. Phys. Fluids 20: 035110.

[5] Sponfeldner T et al. (2015). On the alignment of fluid-dynamic principal strain-rates with the 3D flamelet-normal in a premixed turbulent V-flame. Proc. Combust. Inst. 35: 1269.

[6] Lipatnikov AN et al. (2015). Unburned mixture fingers in premixed turbulent flames. Proc. Combust. Inst. 35: 1401.

[7] Nishiki S et al. (2002). Modeling of flame-generated turbulence based on direct numerical simulation databases. Proc. Combust. Inst. 29: 2017.

[8] Nishiki S et al. (2006). Modeling of turbulent scalar flux in turbulent premixed flames based on DNS databases. Combust. Theory. Model. 10: 39.